Optimal Pressures and Temperatures for Isobaric, Isothermal Chemical Vapor Infiltration

John Y. Ofori and Stratis V. Sotirchos
Dept. of Chemical Engineering, University of Rochester, Rochester, NY 14627

This study addresses the possibility of identifying optimal pressure and temperature pairs that can be used to give the least processing time during isobaric isothermal chemical-vapor infiltration (CVI) within a window of operating conditions. Optimal pressure–temperature pairs are determined as the solution of an optimization problem that seeks to minimize the processing time predicted by a CVI model under the constraint that the maximum density difference in the preform at the end of the densification does not exceed a preset limit. Results are presented on the dependence of the optimum processing time on the type of structure of the preform, the specifications that the final product has to conform to, and the kinetics of the chemical reaction. The results show that operation at low pressure affects adversely the processing time and that a dramatic reduction in the processing time can be achieved by operating in the vicinity of the optimal pressure.

Introduction

Chemical vapor infiltration (CVI) is a method of ceramic or carbon matrix composite fabrication in which chemical vapor deposition reactions are employed to deposit the matrix material (ceramic or carbon) on the internal surface of a porous preform. Compared to other methods of composite fabrication, CVI has a number of attractive advantages, among which the most important ones are its ability to fabricate near-net-shape components and deposit a variety of matrices without damaging the material (usually fibers) used for reinforcement, and its flexibility with regard to the number, sizes, and shapes of pieces that it can process simultaneously (Naslain et al., 1992; Chawla, 1993). However, it suffers from the important disadvantage of being a slow and, hence, expensive process, a consequence of the fact that relatively low deposition rates must be employed in order to achieve densification with acceptable density differences between the external surface and the interior of the preform.

In its original formulation and as it is currently being implemented on an industrial scale, CVI is carried out at constant temperature and constant pressure. Under such conditions, the main mechanism of transport of the gaseous reactants in and of the gaseous products out of the preform is diffusion, driven by concentration gradients, usually a slow process. Several approaches have been taken to increase the rate of transport of gaseous reactants and products in the pore space, and, in this way, enable the CVI process to operate at conditions yielding higher reaction rates and, hence, lower processing times, such as high temperatures. Methods investigated along this vein include CVI under conditions of forced flow through the preform without or with a temperature gradient imposed against the pressure gradient (Stinton et al., 1986), CVI under pressure pulsing conditions (Sugiyama and Yamamoto, 1989; Sugiyama and Kurisu, 1992; Sotirchos, 1991, 1993), and CVI in performs heated through volume heating methods such as radio frequency (RF) and microwave heating (Gupta and Evans, 1993; Devlin et al., 1993; Spotz et al., 1993), in which case the temperature tends to increase away from the external surface of the heated object toward the interior.

In a theoretical study of the dynamics of chemical vapor infiltration, Sotirchos (1991) raised the possibility of using a mathematical model of a CVI process to identify optimal temperature- and pressure-variation strategies that would yield the least processing time for a given set of preform characteristics (shape, size, and pore structure) and a given deposition reaction. Process optimization is among the most frequently studied problems in the chemical industry. A number of commercial process-modeling software packages now include optimization modules (Biegler, 1992), and a large volume of work has been presented in the process-engineering

Correspondence concerning this article should be addressed to S. V. Sotirchos.

literature over the years on this topic. However no attempt has thus far been made to determine optimal operating conditions for CVI processes. The usual focus of studies dealing with the theoretical aspects of chemical vapor infiltration is the investigation of the effects of various operational parameters on the behavior of the process, and as a result, readers who are primarily interested in the practical aspects of a specific CVI application find themselves in the position of having to sift through a large volume of information to find some results applicable to their application.

Sheldon and Chang (1993) and Chang et al. (1994) addressed the problem of minimization of processing time in CVI at a fixed temperature or pressure. This problem involves only one degree of freedom (pressure or temperature), and therefore, by treating the uniformity constraint —whatever it may be—as an equation, one can solve for the unknown temperature or pressure, respectively. This parameter value is optimal in the sense that different values will either yield longer reaction times and more uniformity of densification than we need or will not satisfy the constraint. A constraint based on the initial Thiele modulus (Levenspiel, 1972) was used by the authors just cited in their calculations.

In the present work, we examine the optimization of the conventional isothermal isobaric chemical-vapor infiltration process. We minimize the time required to achieve a prescribed level of densification in an initially porous preform subject to a constraint on the maximum nonuniformity allowable inside the preform at the end of the densification. The optimization parameters are the operating pressure and temperature. Porous preforms are described by either randomly overlapping capillaries (for the void space) or randomly overlapping fibers (for the solid phase). The deposition of silicon carbide (SiC) via the decomposition of methyltrichlorosilane (MTS) is used as the model reaction.

Mathematical Model

A detailed mathematical model developed along the lines of the multicomponent transport and reaction model given by Sotirchos (1991) and Sotirchos and Ofori (1996) is used to describe the evolution of densification in time during CVI. This model can be applied to any CVI system, no matter how complex its chemistry is and how many chemical species it involves, since it has been formulated for the general case where n species participate in m chemical reactions. The model consists of the mass-balance equations for the gases and the deposited solid and the equations that describe the coupling of fluxes and pressure gradients in the pore space. An energy balance is not used, since the problem that is addressed is isothermal CVI, and the heat released by the reaction cannot, by itself, cause significant temperature gradients in the preforms.

The mass balances (continuity equations) for the gaseous species, expressed in terms of the partial pressures, p_i, are written:

$$\frac{\partial(\epsilon^e p_i/RT)}{\partial t} + \nabla\cdot N_i = \sum_\rho \nu_{i\rho} R_{v\rho}, \qquad (1)$$

where ϵ^e is the accessible porosity of the porous medium, N_i is the molar flux of species i; R is the ideal gas constant; T is the temperature; and $\nu_{i\rho}$ is the stoichiometric coefficient of species i in reaction ρ. $R_{v\rho}$, the volumetric reaction rate (per unit volume of porous medium) of reaction ρ, is given by

$$R_{v\rho} = \epsilon^e R_\rho \quad \text{or} \quad R_{v\rho} = S^e R_{s\rho}, \qquad (2a,b)$$

with $R_{s\rho}$ being the intrinsic rate of the heterogeneous reaction (per unit area); R_ρ the rate of the homogeneous reaction (per unit volume of gas phase), and S^e the accessible internal surface area (per unit volume of porous medium).

The mass balance for the deposited solid expressed in terms of the fractional filling of the pore space (conversion), ξ, has the form:

$$\frac{\partial \xi}{\partial t} = \frac{v_S}{\epsilon_0} \sum_\rho \nu_{S\rho} R_{v\rho}, \qquad (3)$$

where v_S is the molar volume of the deposited solid; ϵ_0 is the initial porosity of the preform: and $\nu_{S\rho}$ is the stoichiometric coefficient of the solid in reaction ρ. The conversion used in Eq. 3 is defined as $\xi = (\epsilon_0 - \epsilon)/\epsilon_0$, where ϵ and ϵ_0 are the total and initial porosity of the solid, respectively.

The dusty-gas model equations (Mason and Malinauskas, 1983; Sotirchos, 1989) are used to describe the coupling of fluxes, partial pressures, and partial-pressure gradients of the gas species in the porous structures:

$$-\frac{1}{RT}\left(\nabla p_i + \frac{Bp_i}{\mu D^e_{Ki}}\nabla p\right) = \sum_{j\neq i} \frac{x_j N_i - x_i N_j}{\mathfrak{D}^e_{ij}} + \frac{N_i}{D^e_{Ki}}, \qquad (4)$$

where p_i and p are partial pressure of the ith species and the total pressure, respectively; x_i is the mole fraction of the ith species in the gas mixture; $\mathfrak{D}^e_{ij}$ is the effective binary diffusivity of the (i,j) pair; D^e_{Ki} is the effective Knudsen diffusivity of the ith species; and B^e is the effective permeability. The dusty-gas model is strictly valid for homoporous media only (i.e., with uniformly sized pores), but it was shown by Sotirchos (1989) that it provides an excellent approximation for diffusion in heteroporous media as well. The variation of $\mathfrak{D}^e_{ij}$, D^e_{Ki}, ϵ^e, S^e, and B^e with the conversion is determined by the structure of the porous medium. Two parameters that depend only on the structure of the porous medium are used to determine the variation of the $n(n-1)/2$ effective binary diffusion coefficients and the n effective Knudsen diffusion coefficients with the conversion, S_1 and S_2, respectively. These parameters are defined by

$$\mathfrak{D}^e_{ij} = S_1\,\mathfrak{D}^*_{ij}\left(\frac{p^*}{p}\right)\left(\frac{T}{T^*}\right)^{3/2}; \qquad D_{Ki} = S_2 D^*_{Ki}\left(\frac{r}{r^*}\right)\left(\frac{T}{T^*}\right)^{1/2} \qquad (5a,b)$$

where r is the radius of the capillary, r^* is the reference radius, T^* and p^* are references quantities (1,300 K and 1 atm, respectively), and other quantities with the superscript * are taken at these reference conditions. The dependence of S_1, S_2, S^e, ϵ^e, and B^e on the conversion can be determined by experiment or the use of theoretical methods.

Two structure evolution models are used in this investigation. The first is a randomly overlapping capillary model that assumes that the pore space consists of long capillaries of uniform size randomly arranged in space, whereas the other views the solid phase of the porous medium as an assemblage of uniformly sized fibers arranged without directional preference in space. Expressions for S_1, S_2, and B^e in the two types of structures are given in Table 1. The binary diffusivities and viscosities are calculated using the Chapman–Enskog theory (Bird et al., 1960), and an estimated mixture viscosity value of 3.7×10^{-5} kg/(m·s) at 1,300 K is used for the gas mixture.

The partial pressures of the gases at the external surface of the preform are assumed to be maintained constant, that is, external mass-transfer limitations are treated as negligible, and the conversion of the pore space is taken to be initially zero. Since transient effects associated with partial pressure changes last for very short times, it makes no difference what initial conditions are used for the partial pressures for long-term densification experiments.

The reaction system employed is the deposition of SiC from the decomposition of MTS in the presence of hydrogen. MTS is assumed to deposit SiC according to the overall reaction

$$CH_3SiCl_3 \xrightarrow{H_2} SiC + 3HCl. \tag{6}$$

The reaction kinetics given by Brennfleck et al. (1984) are employed in this study. We use

$$R_s = \omega k_{s0} \exp(-E/RT) p_{MTS}, \tag{7a}$$

with

$$k_{s0} = 2.290\times10^{-2}\,\text{kmol/m}^2\cdot\text{s}\cdot\text{atm}; \qquad E = 120\times10^6\ \text{J/kmol},$$

where ω is a multiplicative constant used to vary the reaction rate from that given by Brennfleck et al. (1984). In addition to irreversible kinetics, a reversible kinetic form is used to investigate the effect of reversible kinetics on the optimization of the process, since the deposition of SiC by the decomposition of MTS is known to be inhibited by the formation of HCl (Papasouliotis and Sotirchos, 1993; Loumagne, 1993). The reversible rate expression is assumed to have the form

$$R_s = \omega k_{s0} \exp(-E/RT) p_{MTS} - \omega' k'_{s0} \exp(-E'/RT) p_{HCl}. \tag{7b}$$

We use $k'_{s0} = k_{s0}$ and $E' = E$ and treat ω' as a parameter.

Statement of the Optimization Problem

We seek to determine the optimal temperature and pressure that would minimize the time required to reach a certain conversion at the surface of the preform under the constraint that the center-to-surface conversion ratio at the end of the densification run equals a preset value β. The objective function, the time required to raise the surface conversion from an initial level ξ_{s0} to a final level ξ_{sf}, is defined by the expression

$$t_f = \frac{\epsilon_0}{v_S} \int_{\xi_{s0}}^{\xi_{sf}} \frac{d\xi_s}{(R_v)_s}. \tag{8}$$

Table 1. Equations for Structural and Transport Properties

Randomly Overlapping Capillary Structure*

$$r = r_0 \left(\frac{\ln(1-\epsilon)}{\ln(1-\epsilon_0)} \right)^{1/2}$$

$$\epsilon^e = \epsilon = \epsilon_0(1-\xi)$$

$$S^e = S = -\frac{2(1-\epsilon)}{r}\ln(1-\epsilon)$$

$$S_1 = \frac{\epsilon}{\eta^b}$$

$$S_2 = \frac{\epsilon}{\eta^K}\frac{r}{r^*}$$

$$B^e = \frac{\epsilon}{8\eta^v}\left(\frac{r}{r^*}\right)^2$$

$$\eta^b = \eta^K = \eta^v = 3$$

Randomly Overlapping 3-D Fiber Structure

$$r = r_0 \left(\frac{\ln \epsilon}{\ln \epsilon_0} \right)^{1/2*}$$

$$\epsilon^e = \epsilon = \epsilon_0(1-\xi)^*$$

$$S^e = S = -\frac{2\epsilon}{r}\ln \epsilon^*$$

$$S_1 = \frac{\epsilon}{\eta^b};\ \eta^b = \eta^b_{\max}\left(\frac{\epsilon_{\max}-\epsilon_p}{\epsilon-\epsilon_p}\right)^{\alpha};\ \epsilon_p = 0.037$$

If $\epsilon > 0.4$, then $\epsilon_{\max} = 1.0$, $\eta^b_{\max} = 1.000$, $\alpha = 0.661$

If $\epsilon < 0.4$, then $\epsilon_{\max} = 0.4$, $\eta^b_{\max} = 1.906$, $\alpha = 0.965$

$$S_2 = \frac{\epsilon}{\eta^K}\frac{\bar{r}}{r^*};\ \eta^K = \eta^K_{\max}\left(\frac{\epsilon_{max}-\epsilon_p}{\epsilon-\epsilon_p}\right)^{\alpha}$$

$$\epsilon_{\max} = 1.0,\ \eta^K_{\max} = 1.444,\ \alpha = 0.921^{**}$$

$$B^e = \frac{\epsilon^e}{8\eta^v}\left(\frac{\bar{r}}{r^*}\right)^2;\ \eta^v = \eta^b;\ \bar{r} = \frac{2\epsilon}{S}$$

*Sotirchos (1987, 1991).
**Tomadakis and Sotirchos (1993).

The constraint on the optimization problem, that the center-to-surface conversion ratio at the end of the densification should equal or be greater than a specified value β, is expressed by

$$\frac{\xi_{cf}}{\xi_{sf}} \geq \beta = \frac{1}{\xi_{sf}} \int_{\xi_{s0}}^{\xi_{sf}} \frac{(R_v)_c}{(R_v)_s}\, d\xi_s. \tag{9}$$

An alternative way of defining the nonuniformity constraint is

$$\frac{\xi_{\text{avg}}}{\xi_{sf}} \geq \beta = \frac{1}{V_p \xi_{sf}} \int_{V_p} \xi\, dV, \tag{10}$$

where V_p is the preform volume. Note that in all our results, the conversion decreases monotonically from the surface to the center of the preform, and thus the center-to-surface conversion ratio is always smaller than the ratio of the conversion at any other spatial position to the conversion at the

surface of the preform. In presenting our results, we give the time in dimensionless form (τ), which is defined as

$$\tau = \frac{1}{10}\left(\frac{t}{t_{\max}}\right);$$

$$t_{\max} = \frac{r_0^*}{\upsilon_S \omega^* k_{s0} \exp\left(\frac{-E}{RT^*}\right) p^*_{\mathrm{MTS},b}}, \quad (11a,b)$$

where all quantities with the superscript * are reference quantities ($r_0^* = 50$ μm; $T^* = 1{,}300$ K; $p^*_{\mathrm{MTS},b} = 0.1$ atm; $\omega^* = 1$), and $t_{\max}$ is the time required to fill a pore of radius 50 μm when the reaction takes place at the reference conditions.

The optimization problem that is defined by Eqs. 8 and 9 (or Eqs. 8 and 10) can be solved using standard solution methods (Beveridge and Schechter, 1970; Ray and Szekely, 1973; Reklaitis et al., 1983; Pike, 1986). It should be noted that if only one operating parameter is allowed to change, that is, pressure or temperature, then this problem can be solved to determine the value that satisfies the constraint. This can always be done if the pressure is fixed and the temperature is varied, because the temperature affects strongly the reaction rate. However, the reverse is not true since the pressure affects only the intraparticle diffusion coefficient, and even then, only if diffusion occurs in the transition or bulk diffusion regime (Sotirchos, 1991).

In this study we determine pressure and temperature pairs (p,T) that minimize the densification time subject to the constraint defined in Eq. 9. We examine the effect of structural, kinetic, and processing parameters on the optimal times and conditions (p,T). We also study the effect of the level of complexity built into the mathematical model on the optimal results. It should be pointed out that since the upper limit of the time horizon is now variable—it is the value of the objective function—the conversion at the surface, ξ_s, is used as a timelike variable instead. The optimization problem was solved by using the secant method, in conjunction with the complete CVI model, to determine temperature values that would satisfy the constraint at a selected pressure. Brent's method (Press et al., 1992) was then employed to minimize the time with respect to pressure (with each pressure having associated with it a temperature satisfying the nonuniformity constraint). The CVI model was solved using piecewise polynomial approximation of the partial pressure and conversion profiles, followed by collocation, and numerical differentiation of the dusty-gas model equations to determine $\nabla\cdot\boldsymbol{N}_i$. This treatment led to a set of algebraic and ordinary differential equations, which was solved in time using a Gear-type solver (Gear, 1971). More details of the solution method for the CVI model are given by Sotirchos (1991).

Results and Discussion

Qualitative results for a simple flux model

Before we discuss the various results obtained on optimal operating conditions and processing times, we present a qualitative discussion of the optimization of isobaric isothermal CVI using a simple diffusion flux model of the Fick's law form. This qualitative discussion can be followed with greater ease by people who are not familiar with the details of transport and reaction in porous media, and it also shows that the conclusions reached are valid no matter what the actual kinetics of the process are.

Under isobaric and isothermal conditions and with Fick's law used to describe the diffusion of each species in the pore space of the preform, the mass balance for the ith species at pseudosteady state can be written as

$$\nabla\cdot\left(\frac{p}{RT} D_i^e(p,T)\frac{dx_i}{dz}\right) + \nu_i R_s(p,T,\boldsymbol{x}) S^e = 0, \quad (12)$$

where $\boldsymbol{x}$ is the vector of mole fractions. Application of the Gauss theorem to Eq. 12 for reactant R ($\nu_R = -1$) gives

$$\left(\frac{p}{RT} D_R^e(p,T)\frac{dx_R}{dz}\right)_s S_p = \int_{V_p} R_s(p,T,\boldsymbol{x}) S^e \, dV, \quad (13)$$

where x_R is the mole fraction of R; $D_R^e(p,T)$ is the effective diffusion coefficient of R; p/RT is the concentration; S_p is the external surface area of the preform; and the subscript s refers to the external surface.

In order to have insignificant density differences (β close to 1), $\boldsymbol{x}$ in the interior should not be much different from the value at the surface, $\boldsymbol{x}_s$. The same would also be the case with S^e, $D_R^e(p,T)$, and $R_s(p,T,\boldsymbol{x})$. Using this observation, we can solve Eq. 13 for $(R_v)_s = S^e R_s(p,T,\boldsymbol{x}_s)$, and use Eq. 8 to derive an expression for the final densification time involving the product $[(p/RT)D_R^e(p,T)^{(dx_R/dz)}]_s$. We have for slab geometry

$$t_f = \frac{a\epsilon_0}{\upsilon_S}\int_{\xi_{s0}}^{\xi_{sf}} \frac{d\xi_s}{\left[\frac{p}{RT} D_R^e(p,T)\frac{dx_R}{dz}\right]_s}. \quad (14)$$

It follows from Eq. 14 that in order to reduce the processing time we must increase the product $[(p/RT)D_R^e(p,T)^{(dx_R/dz)}]_s$, that is, increase the rate at which the reactant enters the preform. This can be done by increasing the diffusion coefficient, the total concentration in the gas phase (or equivalently the pressure), or the mole fraction gradient of R. The extent of nonuniformity of deposition in the interior is determined by how far $\boldsymbol{x}$ in the interior is from the surface values, $\boldsymbol{x}_s$. This is in turn determined by the gradient at the surface, $(dx_R/dz)_s$ for the reactant R. Given the composition of the gas phase and the maximum density gradients that can be tolerated in the final product, $(dx_R/dz)_s$ is fixed in an average sense; therefore the flux of R at the external surface, and hence the processing time can be changed only by varying the factor $D_R^e(p,T)p/RT$.

The range in which the temperature can be varied is rather limited, and besides, the effect of temperature on the effective diffusion coefficient is rather small. The pressure, on the other hand, can be changed over more than two orders of magnitude, and it affects strongly $D_R^e(p,T)$, especially in the high-pressure range where the process is in the bulk-diffusion regime and molecule–molecule collisions dominate. However, the product $D_R^e(p,T)p/RT$ decreases with decreas-

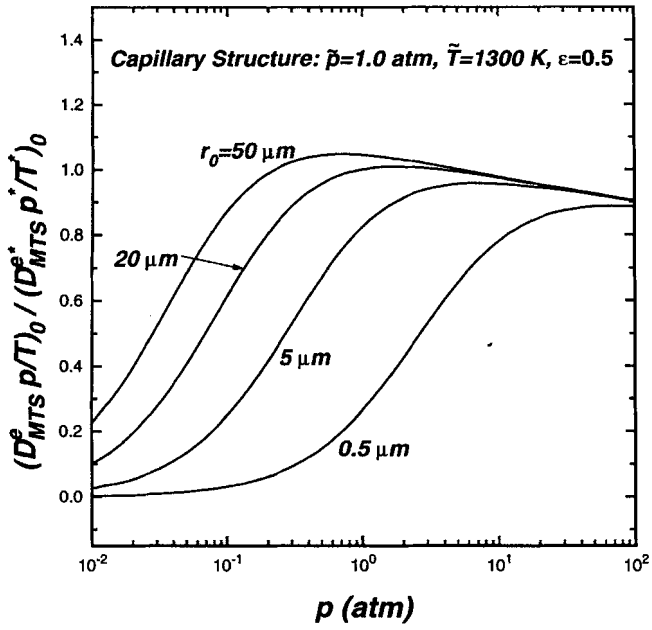

Figure 1. Effect of pressure on $D^e(p,T)p/RT$ in capillary structures.

$\epsilon_0 = 0.5$; $a = 0.01$ m; $x_{MTS} = 0.1$; $x_{H_2} = 0.9$; $\omega^* = 1.0$; $p^* = 1$ atm; $T^* = 1{,}300$ K; $r^* = 20$ μm.

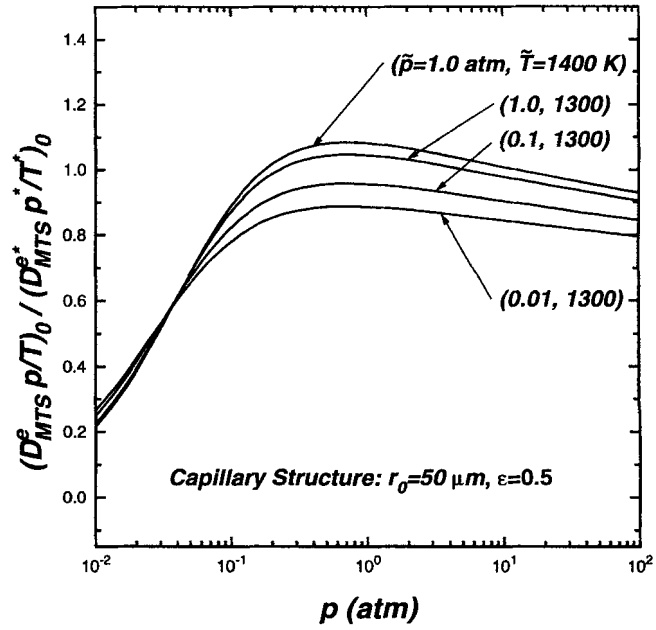

Figure 2. Effect of pressure on $D^e(p,T)p/RT$ in a capillary structure at various deposition rates (parameters same as in Figure 1).

ing pressure, and as a result, a decrease in pressure leads to a decrease in the flux (see Eq. 12) and an increase in the processing time. This effect becomes more pronounced at low pressures and for small pore sizes, where $D_R^e(p,T)$ becomes independent of pressure; as a result, the flux decreases proportionally to pressure, and the processing time increases in inverse proportion to pressure.

Some results on the variation of the $D^e(p,T)p/RT$ factor with pressure are shown for various pore sizes in Figure 1 for MTS diffusing in hydrogen. In all cases the effective diffusivity D_{MTS}^e is calculated using the Bosanquet formula (Pollard and Present, 1948)

$$\frac{1}{D_{MTS}^e} = \frac{1}{\mathfrak{D}_{MTS,H_2}^e} + \frac{1}{D_{K,MTS}^e}, \qquad (15)$$

$D^e(p,T)p/RT$ values are given in dimensionless form, with the value for a capillary structure with a uniform radius of 20 μm at 1 atm and 1,300 K used as reference. All curves shown in Figure 1 were constructed by varying the temperature—decreasing it with increasing pressure—in order to keep the deposition rate [i.e., $\exp(-E/RT)px_{MTS}$] constant and equal to that at $\tilde{p}$ and $\tilde{T}$ (1 atm and 1,300 K). It follows from Eqs. 5a, 5b and 15 that $D^e(p,T)p/RT$ increases monotonically with the pressure at constant temperature; specifically, it is proportional to pressure in the Knudsen regime and independent of it in the ordinary diffusion regime. On the other hand, it decreases with the temperature in the Knudsen regime (varies proportionally to $T^{-1/2}$) and increases in the ordinary diffusion regime (varies proportionally to $T^{1/2}$). Since the temperature decreases with the pressure in Figure 1, a maximum is exhibited by all curves in the vicinity of the ordinary diffusion regime. If the effect of temperature on $D^e(p,T)p/RT$ were ignored, the maximum would obviously be located at the infinite-pressure limit. Since the transition from Knudsen to ordinary (bulk) diffusion occurs at higher pressures with decreasing pore size, the location of the maximum moves toward larger pressures as the capillary size becomes smaller, and the maximum itself decreases.

The variation of the quantity $D^e(p,T)p/RT$ with the pressure at different deposition rates is shown in Figure 2. The deposition rate in each case (each curve) is that obtained at the values of temperature and pressure $(\tilde{p},\tilde{T})$ associated with it. The behavior of the various curves of Figure 2 is qualitatively similar to that discussed earlier for those of Figure 1. Figure 3 shows the temperatures that correspond to the pressures in each of the curves in Figure 2. (The temperatures in some of the curves of Figure 3 in the extreme regions of the pressure range are unreasonably high or low compared to the temperatures used in practice, but they were retained for the sake of completeness of the presented results.) It is seen in Figure 3 that the temperature increases with increasing deposition rate at each pressure for the results shown in Figure 2. Since the effect of temperature on $D^e(p,T)p/RT$ changes from negative to positive as the dominant mode of diffusion changes from Knudsen to bulk, $D^e(p,T)p/RT$ increases with increasing deposition rate at high pressures (bulk-diffusion regime and upper part of the transition regime) and decreases at low pressures. The maximum value of $D^e(p,T)p/RT$ occurs at similar pressure values for all deposition rates, and this is not unexpected considering that the pore size is the same in all cases. However, the temperature value that corresponds to the maximum (compare Figures 2 and 3) shows considerable variation with the deposition rate.

Figure 4 shows the effect of the progress of densification on the evolution of the $D^e(p,T)p/RT$ vs. p relationship at fixed deposition rate for a preform with initial capillary size

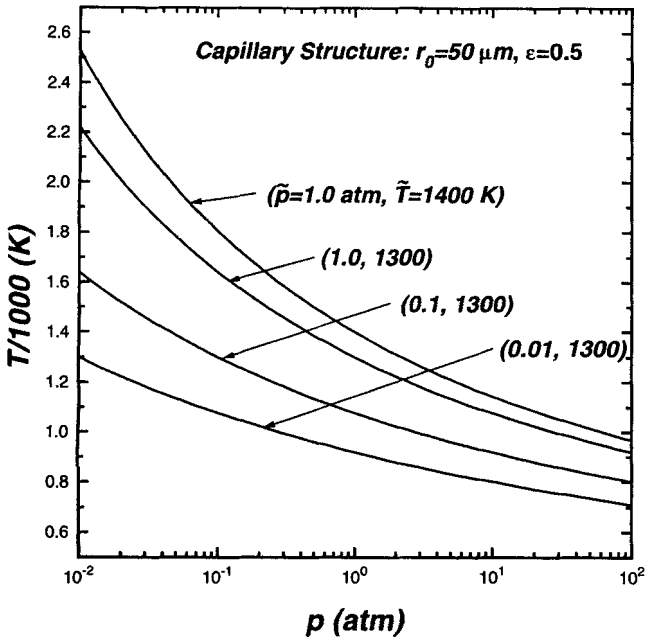

Figure 3. Variation of temperature with pressure at various deposition rates in a capillary structure (parameters same as in Figure 1).

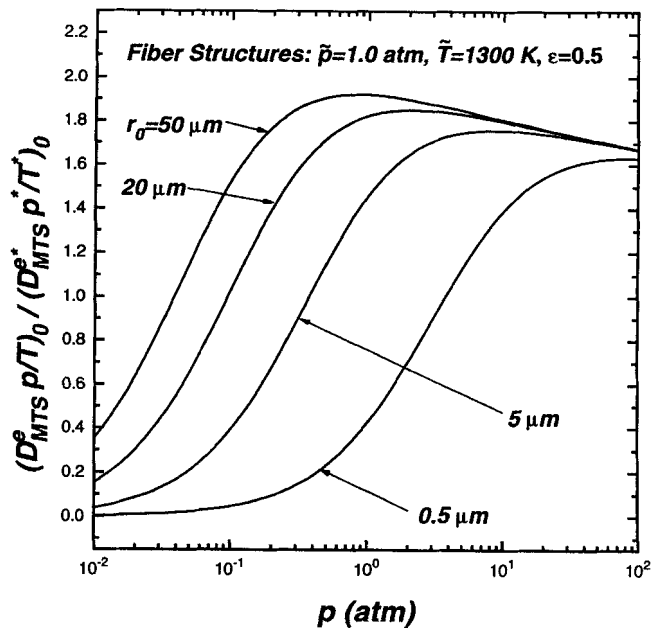

Figure 5. Effect of pressure on $D^e(p,T)p/RT$ in fiber structures with various pore sizes (parameters same as in Figure 1).

(radius) equal to 50 μm. It is seen that the optimal pressure moves toward higher pressures as higher densification levels are reached. This is due to the reduction in pore size with densification, and it essentially corresponds to the effect seen in Figure 1. However, the values of $D^e(p,T)p/RT$ for large values of ξ in Figure 4 are much smaller than those for small values of pore size in Figure 1 at the same pressure, because in Figure 1 the porosity, and hence the effective diffusivity, is much larger.

The behavior of $D^e(p,T)p/RT$ with varying pressure in a 3-D fiber structure is shown in Figures 5 and 6, which are equivalent to Figures 1 and 4 for the capillary structure. The various curves in Figures 1 and 5 behave similarly, but the absolute values of $D^e(p,T)p/RT$ are larger for the fiber

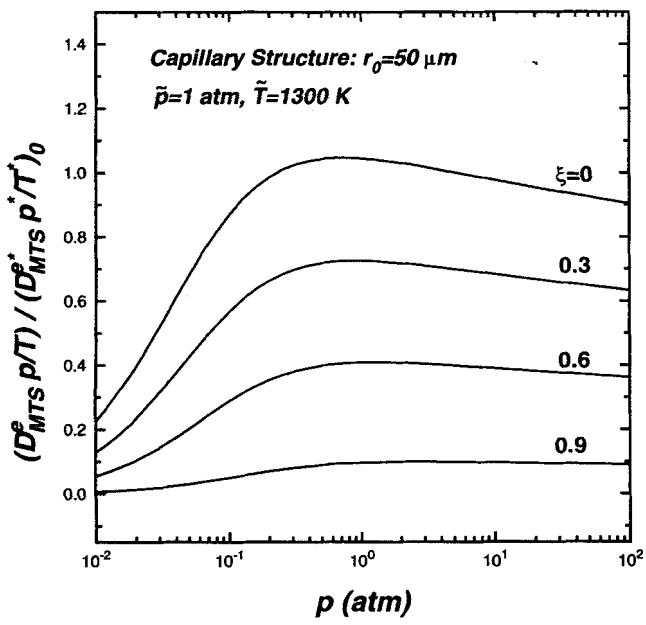

Figure 4. Effect of pressure on $D^e(p,T)p/RT$ in a capillary structure at different conversions (parameters same as in Figure 1).

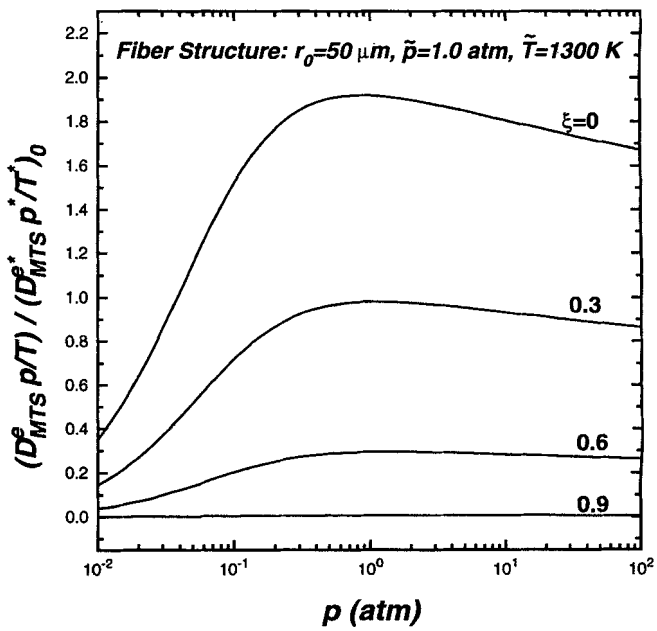

Figure 6. Effect of pressure on $D^e(p,T)p/RT$ in a fiber structure at varying conversions (parameters same as in Figure 1).

structure than for the capillary structure. Also, the pressure at which the maximum occurs is slightly higher in the fiber structure. The first observation is explained by the fact that at a porosity of 0.5 the capillary structure has smaller Knudsen and bulk diffusivities than the fiber structure. The second observation reflects the fact that the transition from the bulk to the Knudsen regime (with decreasing pressure) depends on the relative magnitudes of $\mathfrak{D}_{ij}^e$ and D_{Ki}^e and occurs at higher pressures in the fiber structure at intermediate porosity levels (see Table 1). For the same reason, the region in which the curves in Figure 2 intersect each other was found to lie at higher pressures in the case of fiber structures (Ofori, 1996).

Comparison of Figures 4 and 6—each of these figures shows results for different conversions (or equivalently porosities)—indicates that for ξ values of 0 and 0.3, the curves for the fiber structure (Figure 6) lie above those for the capillaries (Figure 4), while the opposite situation prevails for the higher conversion levels. This difference is the result of the different evolution of the tortuosity factors for bulk and Knudsen diffusion with the porosity in the two types of porous media, capillaries, and fibers (see the equations of Table 1). From the results of Figures 4 and 6 one concludes that for a given level of densification uniformity (i.e., dx_{MTS}/dz), it will be possible to initially employ higher deposition rates in the fiber structures than in the capillary structures at a fixed pressure or at the optimum value. The opposite would be true at high conversions.

Minimum processing times and optimal processing conditions

The effect of pressure on $D^e(p,T)p/RT$ that was seen in Figures 1, 2 and 4 is reflected in the results of Figure 7. This figure presents values for the best processing time (in dimensionless units) that can be achieved at different pressures for different values of nonuniformity tolerance in the final product (β) in a capillary structure. ($\beta = 0.95$ means that only 5% difference in the density between center and surface of the preform can be tolerated.) The processing time shown at each pressure is that obtained when the temperature is chosen so that the uniformity criterion of Eq. 9 is satisfied as an equality. This may be thought of as the best (locally minimum) processing time at the given temperature since a lower reaction temperature will give longer processing times and more uniformity than we are willing to accept, whereas higher temperatures will violate the nonuniformity criterion. The presented results are for a 2-cm-thick preform having 50-μm initial average pore size. It is seen that for all the β values shown, the processing time presents a minimum located within the range 0.4–0.7 atm pressure, well above the 10–50-torr range used in most industrial applications. The optimal processing time is smaller by a factor of 2–3 than the processing time at 10-torr pressure.

The results in Figure 7 can be used to derive conclusions on the effects of the value of the nonuniformity parameter β and of the detail built into the mathematical model on the predicted processing time. As expected, more stringent requirements on the uniformity of deposition lead to larger processing times, with the optimal processing time increasing by a factor of about 3 as the nonuniformity tolerance is

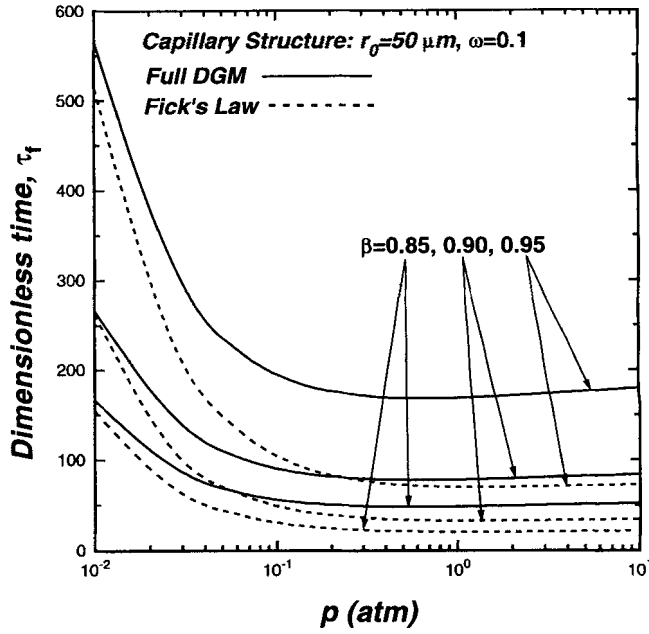

Figure 7. Variation of processing time with operating pressure in a 50-μm capillary structure.

$\epsilon_0 = 0.5$; $a = 0.01$ m; $x_{\mathrm{MTS}} = 0.1$; $x_{\mathrm{H}_2} = 0.9$; $\xi_{sf} = 0.9$; $t = 11{,}458 \cdot \tau$ s.

changed from 15% to 5%. The predicted processing time is also seen to depend strongly on the type of the mathematical model, with the simple model, based on the use of Fick's law for the diffusion fluxes, predicting much smaller processing times than the rigorous multicomponent mathematical model that uses the dusty-gas model to describe the interaction of pressure gradients and diffusion fluxes in the pore space. This difference is mainly due to the fact that the simple model does not account for the negative effect of the product gas (HCl) on the flux of the gaseous reactant toward the center of the preform, and it thus leads to overestimation of the diffusion flux and underestimation of the processing time.

For smaller capillary and fiber sizes (see Figures 1 and 5), the optimal pressures are located at much higher pressures (even above 1 atm), and the difference between the optimal processing time and the best time at the pressures currently used in the industry is much larger than that seen in Figure 7. This observation is particularly important in the densification of carbon matrix composites, where after impregnation of the preforms with resin and pryolysis, the average pore size becomes much smaller than those between the filaments and between the filament bundles in the original preform. Figure 8 shows the densification times obtained for a capillary structure with an initial radius of 20 μm. The minimum densification time in Figure 8, for the cases where the dusty-gas model is used, is slightly larger than the minimum time for the larger-size pores (Figure 7). The best processing time at 10 torr is greater than the optimal time by about a factor of 5–6 in Figure 8, and a factor of 2–3 in Figure 7. Another observation from Figures 7 and 8 is that the optimal pressure increases with decreasing pore, and this is in agreement with the results of Figure 1, which show that the pressure where the maximum value of factor $D^e(p,T)p/RT$ occurs decreases with the pore size.

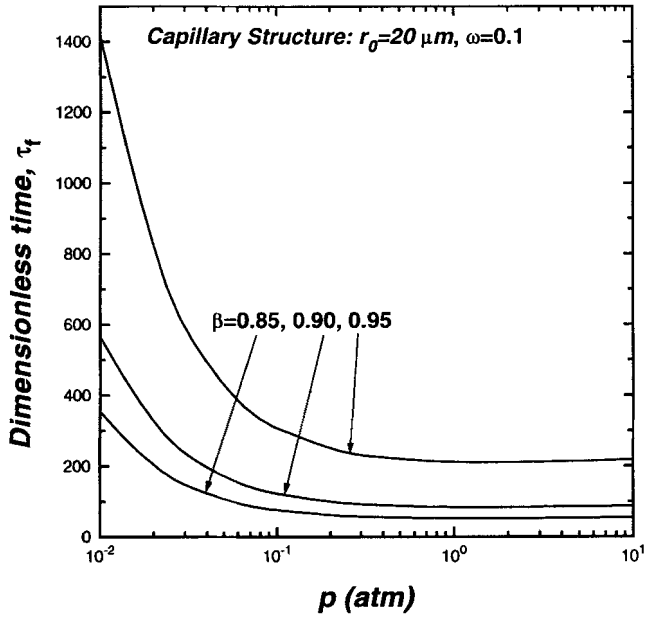

Figure 8. Variation of processing time with operating pressure in a 20-μm capillary structure (parameters same as in Figure 7).

Figure 9 presents the effect of the final conversion at the surface (ξ_{sf}) and of the uniformity tolerance (β) on the minimum processing time for capillary and fiber structures. We saw in Figures 4 and 6 that for a given value of β, higher deposition rates or, equivalently, reactant fluxes at the surface can be tolerated in a fiber structure than in a capillary structure at low values of conversion, whereas at high conversions the opposite is true. Figure 9 shows that the lower "acceptable" reaction rates at high conversions may offset the effect of the initial higher reaction rates in the fiber structures at high surface conversions and lead to higher minimum processing times than those for capillary structures of the same characteristic size. By decreasing the value of the center-to-surface conversion ratio (uniformity parameter β), the effect of low reaction rates at higher conversions on the reaction times diminishes—in as much as high conversions are encountered only close to the external surface of the preform—and as a result, for β smaller than a certain value, the minimum processing time for fibers can become smaller than that for capillaries, even for large surface conversions.

Since the internal surface area, S^e, and the effective mass-transport coefficient change differently, in a relative sense, in the course of densification, and the process is carried out at constant pressure and temperature, the instantaneous center-to-surface reaction rate ratio and the center-to-surface conversion ratio vary with the conversion at the surface. Results on the variation of these two ratios with the surface conversion for capillary and fiber structures during densification at the optimal conditions are shown in Figure 10. It is seen that for the fiber structure, both ratios start from a value higher than β at conversion zero and decrease monotonically with increasing surface conversion, with ξ_c/ξ_s reaching β at the final surface conversion value. This behavior is a consequence of the fact that mass transport becomes slower relative to reaction as densification progresses. (For the simple model this is tantamount to saying that the Thiele modulus, $\Phi^2 = a^2\omega k_s S^e RT/D^e(p,T)$, increases with increasing conversion.) This is also happening in the capillary structure, but we see in Figure 10 that ξ_c/ξ_s and $(R_v)_c/(R_v)_s$ start from a value higher than β at conversion zero, but they both go through a minimum in the medium to high conversion region.

This different behavior is caused by the fact that the internal surface area of a unimodal capillary structure drops faster

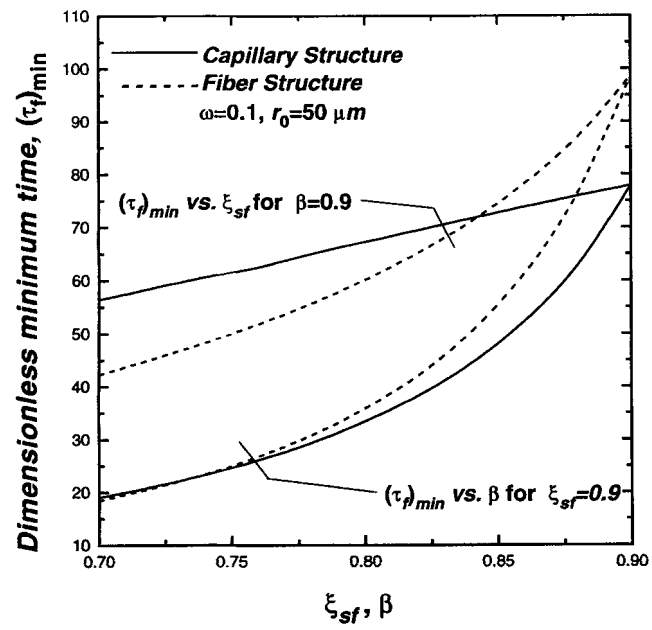

Figure 9. Effect of final surface densification level and nonuniformity parameter on optimal densification times (parameters same as in Figure 7).

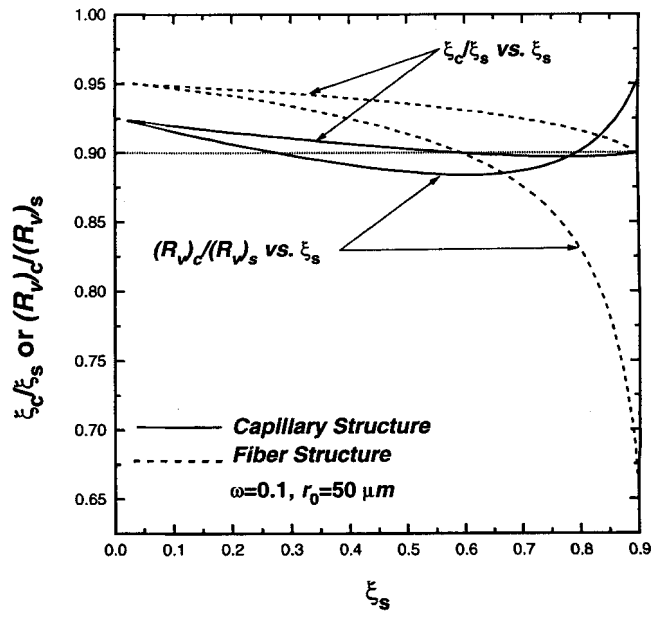

Figure 10. Progress of center-to-surface conversion and center-to-surface reaction-rate ratios with surface conversion (parameters same as in Figure 7).

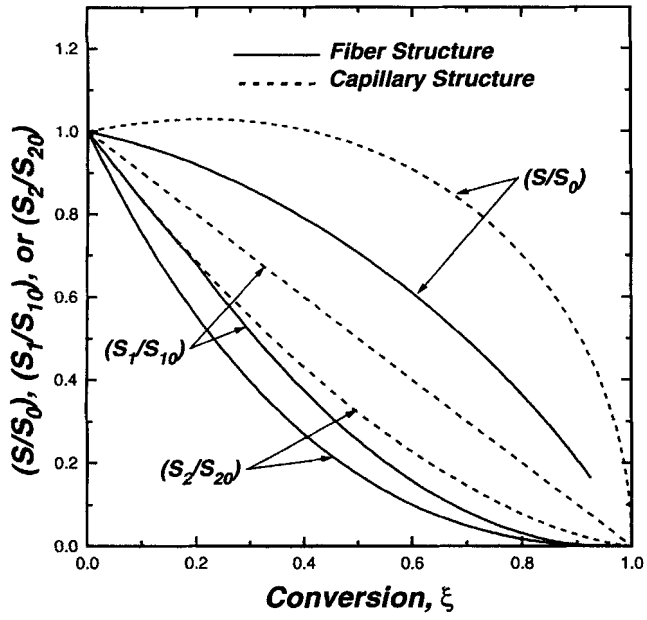

Figure 11. Evolution of normalized structural and transport properties of capillary and fiber structures with conversion.

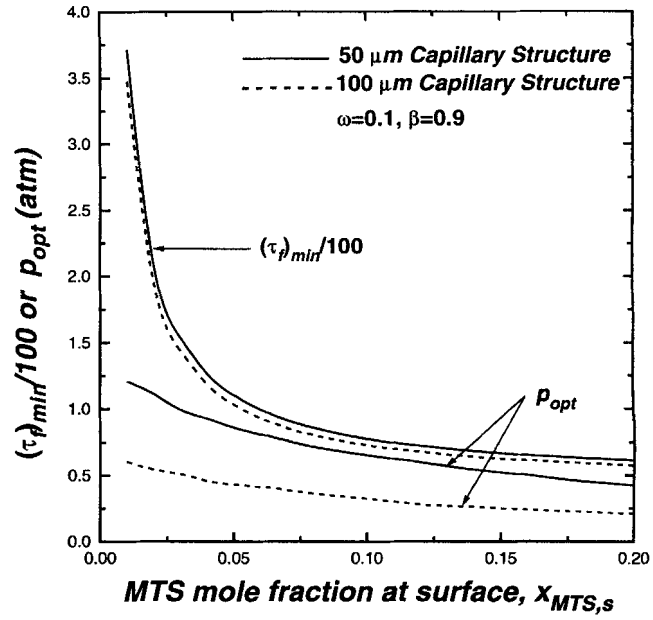

Figure 12. Effect of MTS mole fraction on optimal pressure and densification time.

$\epsilon_0 = 0.5$; $a = 0.01$ m; $t = 11{,}458 \cdot \tau$.

in a relative sense than that of a unimodal fiber structure in the high conversion region. The volumetric deposition rate at the center—where the conversion is lower and the internal surface area higher—can be larger than that at the external surface even though the center concentration is lower. To enable the reader to better follow this argument, as well as other arguments based on the evolution of the internal surface area and the relative resistance of mass transport in the interior of the preform, we show in Figure 11 the variation of the internal surface area, S/S_0, and of the effective bulk and Knudsen diffusivity parameters, S_1/S_{10} and S_2/S_{20}, with the conversion. The normalized Thiele modulus, Φ^2/Φ_0^2, is equal to $(S/S_0)(S_{10}/S_1)$ in the bulk diffusion regime and $(S/S_0)(S_{20}/S_2)$ in the Knudsen regime. The results for the 3-D fiber structure do not exceed conversions of 0.926 because this structure has a percolation threshold of 0.037.

When the simplified CVI model is employed (see Eq. 12), the mole fraction of the reactant for first-order kinetics has no effect on the intraparticle concentration profile for a given structure and a given set of operating conditions. As a result, it does not have any effect on the optimal pressure and temperature of operation as well. However, since the reaction rate is proportional to the mole fraction, the processing time at a given set of operating conditions, and hence the minimum processing time, varies in inverse proportion to it. Results of the dependence of minimum processing time and of the optimal pressure on the MTS mole fraction at the surface ($x_{MTS,s} = x_{MTS,b}$ in the absence of external diffusion limitations) are shown in Figure 12. Even though the kinetic expression used for the deposition rate is linear with respect to MTS, the minimum deposition time does not vary in inverse proportion to the mole fraction, and the optimal pressure does not stay constant. This behavior is caused by the existence of multicomponent interactions among the gaseous species in the reaction mixture, which makes the partial pressure gradient of MTS larger than that predicted by the Fick's law model (see Figure 7).

The effect of these interactions is stronger for larger mole fractions, and this is why the minimum processing time in the upper part of the mole-fraction range decreases with increasing mole fraction less than what the inversely proportional relationship between processing time and mole fraction predicts. For very small mole fractions (p_{MTS}, $p_{HCl} \ll p_{H_2} \approx p$), the multicomponent interactions can be neglected, and the dusty-gas model equations (Eq. 4) give for MTS

$$\frac{1}{RT}\left(\nabla p_{MTS} + \frac{p_{MTS}}{D^e_{K,MTS}}\frac{B^e}{\mu}\nabla p\right) = N_{MTS}\left(\frac{1}{\mathfrak{D}^e_{MTS,H_2}} + \frac{1}{D^e_{K,MTS}}\right). \quad (16)$$

The second term in the lefthand side of Eq. 16 is the contribution of viscous flow. This term is of the order of p^2_{MTS}—∇p is of the order of p_{MTS}—and can be neglected for small p_{MTS} values. Therefore, as the limit of zero mole fraction is approached, the dusty-gas model becomes identical to the Fick's law model. Thus, for mole fractions below 0.01, the optimal pressure tends to level off, and the processing time varies almost inversely proportional to the mole fraction.

The optimal pressure in Figure 12 decreases with increasing mole fraction because the increasing importance of multicomponent interactions makes the effective resistance for transport of MTS in the pore space to deviate progressively from that predicted by the Fick's law model. Thus, the value of the optimal pressure has to be lowered from the optimal value for the Fick's law model in order to weaken the effects of multicomponent interactions and thus satisfy the nonuni-

formity criterion. The two pore sizes exhibit the same qualitative behavior. In agreement with the results of Figures 1, 7, and 8, both the optimal pressure and the minimum processing time decrease with increasing pore size, but the effects on the latter is much weaker. Equation 9 may be used to explain the weak dependence of minimum processing time on the pore size. Since the optimal processing conditions are close to the bulk-diffusion regime, $D^e(p,T)p/RT$ is practically independent of pore size, whereas the average value of $(dx_R/dz)_s$ is determined by the uniformity criterion.

Kinetic effects on optimal processing conditions

We now investigate the dependence of the minimum processing time and of the optimal pressure and temperature on the kinetics of the deposition reaction. The effect of the magnitude of the rate constant, represented by the parameter ω for an irreversible reaction, is considered first. Processing time vs. pressure results are shown in Figure 13 for unimodal capillary structures with 50-μm initial pore radius. Qualitatively similar results are obtained for other pore sizes and for fiber structures (Ofori, 1996). The optimal pressure for each ω is that at the minimum of the corresponding τ_f vs. p curve. For pressures lower than a certain limit the best processing time tends to decrease with increasing rate constant, and the opposite behavior is observed at higher pressure. This behavior is entirely analogous to that seen for the evolution of the $D^e(p,T)p/RT$ vs. p relationship with changing surface relativity [i.e., changing $p \exp(-E/RT)$ factor]. Again, the pressure range where the various curves intersect each other lies in the vicinity of the pressure value where the effect of temperature on the effective resistance for MTS transport in the pore space changes from positive to negative. Since the minimum processing time is found in the high-pressure range (in the bulk-diffusion regime), its value increases with increasing reaction-rate constant, but not by a large, relative to the change of ω, factor.

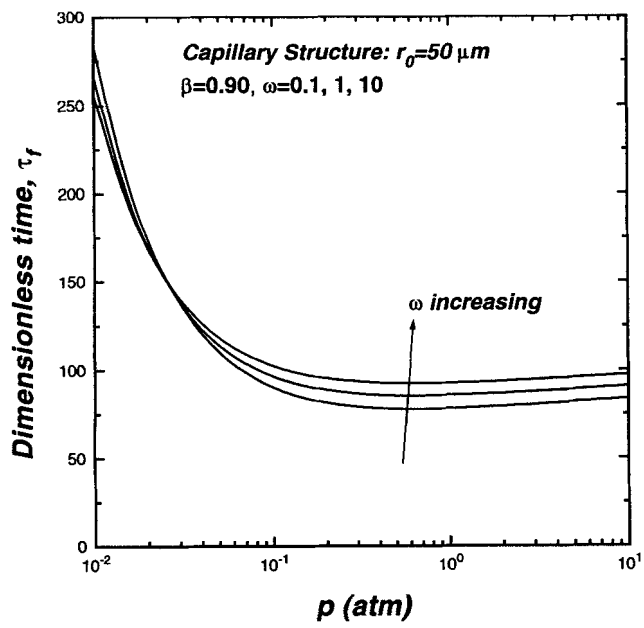

Figure 13. Effects of reaction-rate constant on processing time vs. operating pressure in a 50-μm capillary structure (parameters same as in Figure 7).

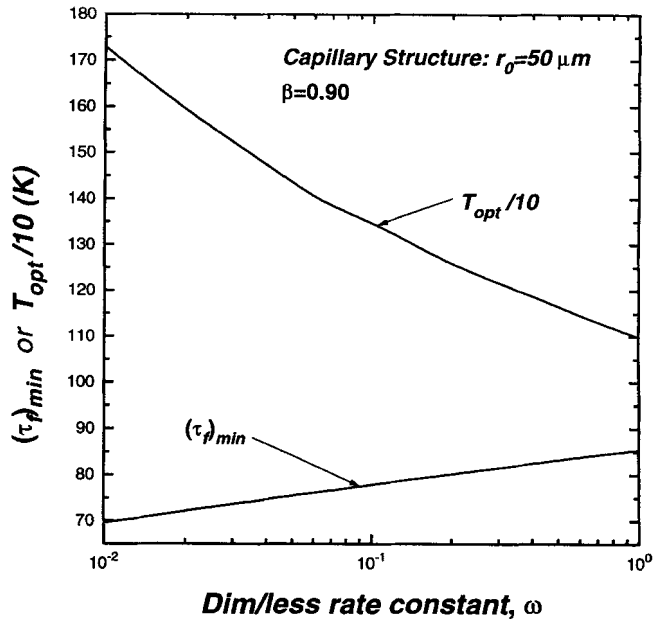

Figure 14. Effect of dimensionless reaction rate constant on optimal temperature and densification time (parameters same as in Figure 7).

The optimal pressure does not change significantly with a change in the reaction-rate constant, and this result agrees well with the behavior of the pressure corresponding to the maximum value of the $D^e(p,T)p/RT$ factor in Figure 2. Figure 14 shows that the optimal temperature decreases significantly as the preexponential factor of the reaction is varied over an interval of two orders of magnitude. Specifically, whereas the optimal pressure changes in the 0.62–0.67-atm range, the temperature decreases from about 1725 K at $\omega =$ 0.01 to 1,100 K at $\omega = 1$. The dependence of the optimal processing conditions on the reaction-rate constant can be explained by considering the effect of temperature on the process parameters. If the effect of temperature on the transport properties is neglected, different (ω,T) combinations yielding the same value of rate constant [i.e., $\omega \exp(-E/RT)$] would produce identical infiltration results. The effect of the temperature on the transport properties is rather weak in comparison to that on the rate constant, and therefore, as ω is increased, T decreases in order to keep $\omega \exp(-E/RT)$ approximately constant and, thus, satisfy the uniformity criterion. In the Knudsen regime, a decrease in T leads to an increase in the transport properties and, on that account, to a decrease in the processing time. The opposite situation is encountered for the processing time in the bulk-diffusion regime and for the minimum processing time.

The results of Figures 1–6 on the variation of the $D^e(p,T)p/RT$ factor and of the effects of this variation on the optimal processing conditions also apply when the reversible rate expression given by Eq. 7b, or in fact, any other rate expression, is employed. The uniformity of deposition is again determined by the mole fraction gradient at the surface, $(dx_R/dz)_s$. However, since the reaction product affects the reaction rate,

larger reaction-rate gradients exist in the interior of the preform for the same value of $(dx_R/dz)_s$ in the case of a reversible reaction. Thus, smaller values of $(dx_R/dz)_s$ and, hence, larger values of processing time (see Eq. 14) are needed to satisfy the uniformity criterion for reversible kinetics. The simplified model can be used to obtain an approximate quantitative relationship regarding the effects of the reversibility of the reaction on the processing time. It is shown in reaction engineering texts (e.g., Levenspiel, 1972) that the Thiele modulus of a reversible reaction with first-order kinetics is given by

$$(\Phi^2)_{\text{rev}} = \frac{a^2 k_v^f \left[1 + \left(\frac{k_v^b}{k_v^f}\right)\left(\frac{-\nu_P}{\nu_R}\right)\left(\frac{D_R^e}{D_P^e}\right)\right]}{D_R^e}, \qquad (17)$$

where k_v^f and k_v^b are the forward and reverse rate constants, and subscript P is used to denote quantities referring to the gaseous product (HCl for SiC deposition). (The first step in deriving Eq. 17 is to use Eq. 12 written for the product and the reactant to express the product concentration in terms of the reactant concentration.) Compared to the Thiele modulus of the irreversible reaction, $(a^2 k_v^f/D_R^e)$, Eq. 17 indicates that the net effect of the reversibility of the reaction in the simplified model is to increase the effective reaction rate constant by the factor $1+(k_v^b/k_v^f)(-\nu_P/\nu_R)(D_R^e/D_P^e)$, which becomes $1+3(\omega'/\omega)(D^e_{\text{MTS}}/D^e_{\text{HCl}})$ for the rate expression of Eq. 7b and the stoichiometry of Eq. 6. We saw in the various results that we have presented and discussed thus far that the optimum pressure is found close to the bulk-diffusion regime, where $D^e_{\text{MTS}}/D^e_{\text{HCl}}$ is practically independent of pressure, conversion, and temperature, being almost equal to $\mathfrak{D}^*_{\text{MTS,H}_2}/\mathfrak{D}^*_{\text{HCl,H}_2}$.

The preceding observations lead us to conclude that the simplified model would predict the same operational conditions for reversible reaction and irreversible kinetics if parameter ω in the irreversible problem has the same value as factor

$$\omega\left(1+3\frac{\omega'}{\omega}\frac{\mathfrak{D}^*_{\text{MTS,H}_2}}{\mathfrak{D}^*_{\text{HCl,H}_2}}\right)$$

in the reversible case. As ω is changed for irreversible kinetics (see Figures 13 and 14), the temperature decreases, keeping the $\omega \exp(-E/RT_{\text{opt}})$ factor and, therefore, the optimal processing time, almost constant. For reversible linear kinetics, it is the factor

$$\omega\left(1+3\frac{\omega'}{\omega}\frac{\mathfrak{D}^e_{\text{MTS,H}_2}}{\mathfrak{D}^e_{\text{HCl,H}_2}}\right)\exp(-E/RT_{\text{opt}})$$

that is kept almost constant, but the optimal processing time is still inversely proportional to $\omega \exp(-E/RT_{\text{opt}})$, that is, the reaction-rate constant at the external surface. Therefore, as ω and ω' are changed, one expects the minimum processing time to vary almost proportionally to

$$1+3\frac{\omega'}{\omega}\frac{\mathfrak{D}^e_{\text{MTS,H}_2}}{\mathfrak{D}^e_{\text{HCl,H}_2}},$$

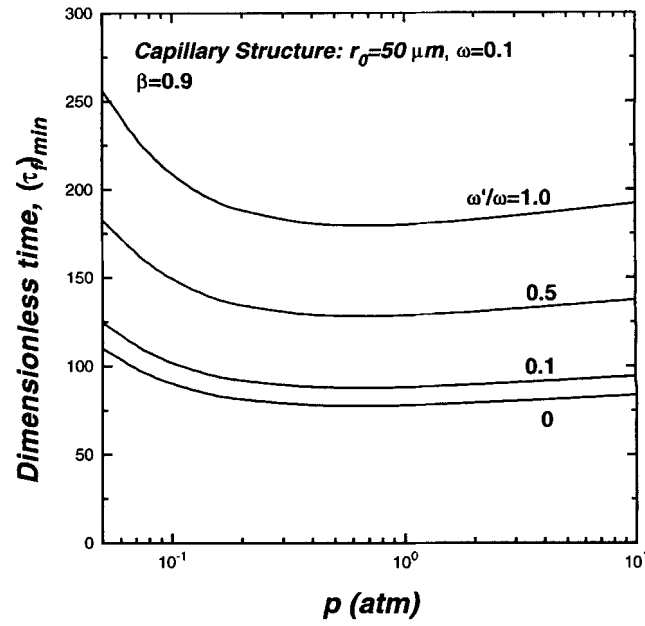

Figure 15. Variation of processing time with operating pressure showing effect of reversibility in a 50-μm capillary structure (parameters same as in Figure 7).

that is, increase almost linearly with ω' for fixed ω, increase slightly with increasing ω (see Figures 13 and 14) for fixed ω'/ω, and vary linearly with $1/\omega$ for fixed ω'. The last result is expected to hold for strongly reversible reactions (large ω' values), since in the irreversible case, $(\tau_f)_{\text{min}}$ increases slightly with increasing ω.

Figure 15 presents processing time vs. pressure results for various ω' values, and Figure 16 shows the variation of the

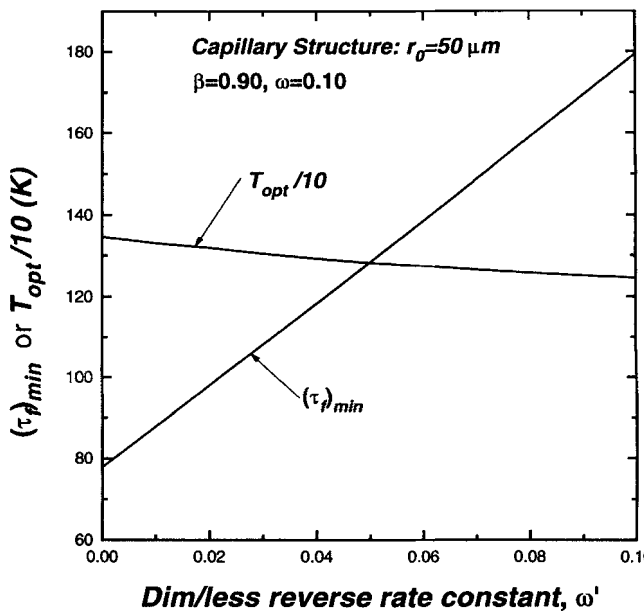

Figure 16. Effect of dimensionless reverse-reaction-rate constant on optimal temperature and densification time (parameters same as in Figure 7).

optimal temperature and of the minimum processing time with ω'. The results shown in these figures are in complete agreement with the observations made in the previous paragraph. The simplified model predicts that the slope of $(\tau_f)_{\min}$ vs. ω' should be equal to 2.5 ($\mathfrak{D}^e_{\mathrm{MTS,H_2}}/\mathfrak{D}^e_{\mathrm{HCl,H_2}} \approx 0.5$), and this value compares very well with the average slope of the $(\tau_f)_{\min}$ vs. ω' curve in Figure 16. The difference is the combined effect of the multicomponent interactions in the complete model used to get the results of Figures 15 and 16 and the fact that even in the simplified model, the slope is not exactly equal to

$$1+3\frac{\omega'}{\omega}\frac{D^e_{\mathrm{MTS,H_2}}}{D^e_{\mathrm{HCl,H_2}}}.$$

In the simplified model, the optimal conditions are determined only by the factor

$$\omega\left(1+3\frac{\omega'}{\omega}\frac{\mathfrak{D}^e_{\mathrm{MTS,H_2}}}{\mathfrak{D}^e_{\mathrm{HCl,H_2}}}\right).$$

Comparison of the optimal temperatures of Figure 16 for $\omega = 0.1$ and ω' between 0 and 0.1, and Figure 14 for ω between 0.1 and 0.25—recall that $\mathfrak{D}^e_{\mathrm{MTS,H_2}}/\mathfrak{D}^e_{\mathrm{HCl,H_2}} \approx 0.5$—shows that this is approximately the case even for the complete model.

We have employed the same preform size to obtain all the results we presented and discussed in this study because the effect of a^2 on the optimal processing conditions is similar to that of ω. To prove this we can use the expression for Thiele modulus of the reversible reaction (Eq. 17). Increasing a^2 by a certain factor is equivalent to applying the same relative increase to ω. In analogy to what happens in the reversible reaction case when ω' is changed, $a^2\omega \exp(-E/RT_{\mathrm{opt}})$ remains approximately constant as a^2 is changed. Thus, the minimum processing time, which is inversely proportional to $\omega \exp(-E/RT_{\mathrm{opt}})$, varies proportionally to a^2. This approximate result can also be obtained from Eq. 14 by realizing that a given value of β fixes the average value of $a(dx_R/dz)_s$, that is, the average mole-fraction gradient of the reactant with respect to the dimensionless distance.

Summary and Concluding Remarks

In this study we determined optimal pressure and temperature pairs (p,T) that minimize the time required to densify by chemical vapor infiltration (CVI) under isobaric, isothermal conditions a porous preform to a prespecified density level at its external surface under the constraint that the uniformity of deposition, measured by the center-to-surface conversion ratio, does not fall below a certain value. A general mathematical model was used to describe the CVI process. It uses the dusty-gas model equations to relate the fluxes of the gaseous species to partial pressure and partial-pressure gradients, with D'Arcy's law employed to describe viscous flow. The structure of the porous medium was represented by randomly overlapping capillaries (for the void space) or randomly overlapping fibers (for the solid phase). The deposition of SiC from MTS was used as a model chemical-vapor infiltration reaction.

A simplified CVI model, based on using Fick's law to describe the transport of each species in the pore space, was used to obtain some general qualitative results on optimal pressures and temperatures in isothermal, isobaric CVI, which were comapred with the numerical results obtained using the general CVI model for SiC infiltration. The results showed that the optimal pressures for CVI under conditions of diffusion-driven transport are much larger than the pressures that are commonly used in industrial CVI processes, lying in the 0.5–0.7-atm range for 50-μm initial pore radius. The minimum densification times that can be achieved at the optimum pressures can be by almost an order of magnitude lower than the best processing times in the 10–50-torr range for 10-μm pores. In general, the optimal pressure is located close to the bulk-diffusion regime, and as a result, it tends to increase with decreasing pore size. The minimum processing time increases slightly as the initial pore size is decreased, but its difference from the best processing time at low pressure varies almost linearly with the inverse of the pore size.

The location of the optimal pressure is affected rather insignificantly by the other parameters of the process, but exactly the opposite situation is observed for the optimal temperature, T_{opt}. T_{opt} decreases significantly with increasing deposition uniformity in the final product, final conversion level at the external surface, reverse reaction-rate constant, and preform size. As a consequence of the decrease in the optimal temperature, the minimum processing time increases significantly in all these cases. The optimal temperature also decreases with increasing forward reaction-rate constant, but in this case, the effect of decreasing temperature is compensated by that of the increased rate constant, and thus, the minimum processing time increases only slightly or even decreases for strongly reversible reactions. The ambient value of the mole fraction of the reactant does not affect strongly the optimal operating conditions, but, since the reaction rate and the rate of mass transport are proportional to it, it has a strong influence on the processing time.

The simplified model was employed to derive an approximate relationship for the variation of the minimum processing time with several of the parameters of the process. These relationships were obeyed rather closely by the results of the general model, but because of multicomponent interactions among the various species in the reacting mixture, the simplified model gave much lower processing times. The type of the pore structure had significant quantitative effects on the predictions of the overall CVI model. Because of smaller diffusion coefficients at high conversions, fiber structures gave larger minimum processing times for higher values of final surface conversion than capillary structures of the same initial porosity and internal surface area.

When the pressure or temperature of operation is fixed, the problem displays only one degree of freedom, and thus, by treating the uniformity criterion as an equality, we can solve for the value of the free parameter. One may use these results to construct processing time vs. p or processing time vs. T curves, and determine the optimal processing conditions as those corresponding to the minimum of those curves. In the processing time vs. p curve, the processing time tends to rise sharply only in the Knudsen diffusion regime, whereas in the bulk diffusion regime where the minimum processing time and the optimal pressure are located, the curve is very

flat. This observation, in conjunction with the weak dependence of the optimal pressure on kinetics, preform size, and operating conditions indicates that provided the chemical vapor infiltration process is carried out away from the Knudsen diffusion regime, the exact value of the operating pressure is rather unimportant. There is a whole range of pressure values where one can find a temperature of operation that satisfies the nonuniformity criterion and yields processing times slightly higher than the minimum processing time. A similar argument may be made about the temperature, but in that case one does not have *a-priori* information on which range of temperatures yields processing times close to the minimum value. It should be noted that since in most chemical vapor deposition reactions, deposition of an acceptable product occurs only within a window of operating conditions, the optimum pressure and temperature values predicted for a certain preform may lie outside that window. Of course, in such a case one should work with the combination of feasible temperature and pressure values that gives the least difference from the minimum processing time, for instance, the highest possible pressure if there are no restrictions on temperature.

Acknowledgment

This research was supported by a grant from NSF.

Literature Cited

Beveridge, G. S. D., and R. S. Schechter, *Optimization: Theory and Practice*, McGraw-Hill, New York (1970).

Biegler, L. T., "Tailoring Optimization Algorithms to Process Applications," *Comput. Chem. Eng.*, **17**, Suppl. s81–s95 (1992).

Bird, R. B., W. E. Stewart, and E. N. Lightfoot, *Transport Phenomena*, Wiley, New York (1960).

Brennfleck, K., E. Fitzer, G. Schoch, and M. Dietrich, "CVD of *SiC*-Interlayers and their Interaction with Carbon Fibers and with Multilayered *NbN*-Coatings," *Proc. Int. Conf. on CVD*, M. Robinson et al., eds., The Electrochem. Soc., Pennington, NJ, p. 649 (1984).

Chang, H. C., T. F. Morse, and B. W. Sheldon, "Minimizing Infiltration Times during the Initial Stage of Isothermal Chemical Vapor Infiltration," *J. Mat. Process. Manuf. Sci.*, **2**, 437 (1994).

Chawla, K. K., *Ceramic Matrix Composites*, Chapt. 4, Chapman & Hall, London (1993).

Devlin, D. J., R. P. Currier, R. S. Barbero, and B. F. Espinoza, *Ceram. Eng. Sci. Proc.*, **14**(9/10), 761 (1993).

Gear, C. W., *Numerical Initial Value Problems in Ordinary Differential Equations*, Prentice Hall, Englewood Cliffs, NJ (1971).

Gupta, D., and J. W. Evans, "Mathematical Model for Chemical Vapor Infiltration in a Microwave-heated Preform," *J. Amer. Ceram. Soc.*, **76**, 1924 (1993).

Levenspiel, O., *Chemical Reaction Engineering*, Wiley, New York (1972).

Loumagne, F., "CVD of Silicon Carbide from Methyltrichlorosilane: Homogeneous and Heterogeneous Processes, Microstructure Characterization," PhD Thesis, Univ. of Bordeaux, Bordeaux, France (1993).

Mason, E. A., and A. P. Malinauskas, *Gas Transport in Porous Media: The Dusty-Gas Model*, Elsevier, New York (1983).

Naslain, R., *Ceramic Matrix Composite*, Chapt. 8, R. Warren, ed., Chapman & Hall, Glasgow (1992).

Ofori, J. Y., PhD Diss., Univ. of Rochester, Rochester, NY (1996).

Ofori, J. Y., and S. V. Sotirchos, "Multicomponent Transport in Chemical Vapor Infiltration," *Ind. Eng. Chem. Res.* **35**, 1275 (1996).

Papasouliotis, G. D., and S. V. Sotirchos, "Heterogeneous Kinetics of the Chemical Vapor Deposition of Silicon Carbide from Methyltrichlorosilane," *MRS Symp. Proc.*, Vol. 334, p. 111 (1993).

Pike, R. W., *Optimization for Engineering Systems*, Van Nostrand Reinhold, New York (1986).

Pollard, W. G., and R. D. Present, "On Gaseous Self-diffusion in Long Capillary Tubes," *Phys. Rev.*, **73**, 762 (1948).

Press, W. H., S. A. Teukolsky, W. T. Vetterling, and B. P. Flannery, *Numerical Recipes in Fortran: The Art of Scientific Computing*, 2nd ed., Cambridge Univ. Press, New York (1992).

Ray, W. H., and J. Szekely, *Process Optimization*, Wiley, New York (1973).

Reklaitis, G. V., A. Ravindran, and K. M. Ragsdell, *Engineering Optimization: Methods and Applications*, Wiley, New York (1983).

Sheldon, B. W., and H. C. Chang, "Minimizing Infiltration Times during the Final Stage of Isothermal Chemical Vapor Infiltration," *Ceram. Trans.*, **42**, 81 (1993).

Sotirchos, S. V., "On a Class of Random Pore and Grain Models for Gas-Solid Reactions," *Chem. Eng. Sci.*, **42**, 1262 (1987).

Sotirchos, S. V., "Multicomponent Diffusion and Convection in Capillary Structures," *AIChE J.*, **35**, 1953 (1989).

Sotirchos, S. V., "Dynamic Modeling of Chemical Vapor Infiltration," *AIChE J.*, **37**, 1365 (1991).

Sotirchos, S. V., "Chemical Vapor Infiltration Under Pulsing Conditions, 'High Temperature Ceramic Matrix Composites'," *Proc. 6th European Conf. on Composite Materials*, R. Naslain, J. Lamon and D. Doumeingts, eds., Bordeaux (1993).

Spotz, M. S., D. J. Skamser, P. S. Day, H. M. Jennings, and D. L. Johnson, "Microwave-assisted Chemical Vapor Infiltration," *Proc. Conf. on Advanced Composites and Advanced Ceramic Materials*, Cocoa Beach, FL, p. 753 (1993).

Stinton, D. P., A. J. Caputo, and R. A. Lowden, "Synthesis of Fiber-reinforced SiC Composites by Chemical Vapor Infiltration," *Amer. Ceram. Soc. Bull.*, **65**, 347 (1986).

Sugiyama, K., and E. Yamamoto, "Reinforcement and Anti-oxidizing of Porous Carbon by Pulse CVI of *SiC*," *J. Mat. Sci.*, **24**, 3756 (1989).

Sugiyama, K., and Y. Kurisu, "Pulsed Chemical Vapor Infiltration of TiN into a Fine Capillary Sealed at One End," *J. Mat. Sci.*, **27**, 4070 (1992).

Tomadakis, M. M., and S. V. Sotirchos, "Transport Properties of Random Arrays of Freely Overlapping Cylinders with Various Orientation Distributions," *J. Chem. Phys.*, **98**, 616 (1993).

Manuscript received Sept. 28, 1995, and revision received Feb. 26, 1996.